International Journal of Hydrogen Energy 110 (2024) 687–694

Contents lists available at ScienceDirect

International Journal of Hydrogen Energy

journal homepage: www.elsevier.com/locate/he

# Potential-dependent phase stability and trapped-electrons origin in copper oxide-based photocathodes for water splitting

Xiufang He [a], Tomasz Baran [b], Martina Fracchia [c,e,*], Alberto Visibile [d], Alberto Vertova [a,e,**], Paolo Ghigna [c,e], Alessandro Minguzzi [a,e,f]

[a] Dipartimento di Chimica Università degli Studi di Milano, via Golgi 19, 20133, Milan, Italy
[b] SajTom Light Future LTD, Wezerow 37, 32-090, Slomniki, Poland
[c] Dipartimento di Chimica, Università degli Studi di Pavia, Viale Taramelli 13, 27100, Pavia, Italy
[d] ESAB AB, R&D Filler Metals, Lindholmsallén 9, 417 55, Gothenburg, Sweden
[e] INSTM, Consorzio Interuniversitario per la Scienza e Tecnologia dei Materiali, Via Giusti 9, Firenze, Italy
[f] Dipartimento di Energia, Politecnico di Milano, Via Lambruschini, 4a, 20156, Milano, Italy

ARTICLE INFO

*Keywords:*
Photoelectrochemical water splitting
Copper oxides
EXAFS
XANES
FEXRAV

ABSTRACT

Operando XAS studies in the field of photoelectrochemistry are quite scarce and are mostly devoted to composite systems, rather than to pure semiconductors. However, improving the knowledge of the primary photocatalytic processes occurring in semiconductors, e.g. charge generation, trapping and recombination is crucial to improve the performances of the photoactive materials. In this work, we report a study on the behavior of copper oxide-based photocathodes for hydrogen generation in water splitting. The phase composition of the materials in pristine conditions and after photocorrosion was investigated also considering the role of the applied potential in the dark and under illumination. The fate of the photogenerated carriers during the water splitting reaction was investigated by employing differential XANES spectra in dark and light.

## 1. Introduction

Photoelectrochemical (PEC) and photocatalytic fuel production, in particular hydrogen evolution from water splitting (WS), are attracting enormous interest due to their reported increasing efficiencies [1,2], in light of the reduction of the impact of fossil fuels. Currently, the main research effort in photoelectrochemical water splitting is the development of suitable photoelectrode materials with proper stability and activity.

Improving the knowledge on the primary photocatalytic processes e.g. charge transfer, trapping and recombination is crucial for PEC-WS devices development [3,4]. In this context, the present paper focuses on understanding the behavior of mixed copper oxide materials by X-ray absorption spectroscopy (XAS) under both *ex-situ* and *operando* conditions. O*perando* studies (using an illuminated electrochemical cell under an external bias) are greatly useful because many properties of photoelectrodes are intimately coupled to the features of the liquid-phase electrolyte. Operando investigations enable the direct observation of photoactive materials under irradiation with light and/or the application of a potential [5–10], whereas *ex situ* investigations provide complementary characterizations of the photoelectrodes [11,12]. XAS includes element-specific techniques as XANES - X-ray Absorption Near Edge Structure, EXAFS - Extended X-ray Absorption Fine Structure and FEXRAV - Fixed Energy X-Ray Absorption Voltammetry [13–15], for studying the electronic and atomic structure of matter, in particular oxidation states and local atomic environment [6,16], also for analytical purpose [17].

The existing literature of operando XAS in photoelectrochemistry is quite scarce and it is mostly dedicated to composite systems. For instance, we studied hematite/iridium oxide composites at the Ir-$L_{III}$ edge during the photogeneration of charges in hematite to probe the transfer of electrons and holes between the two layers [5]. Moreover, we synthesized FeNi (oxy)hydroxide co-catalyst overlayer deposited on thin-film hematite ($\alpha$-$Fe_2O_3$) as photoanode and suggested that the holes are photogenerated in $\alpha$-$Fe_2O_3$ and transferred to Ni atoms in the overlayer [18]. We also developed time-resolved, pump and probe hard X-ray absorption spectroscopy in photoelectrochemical conditions under UV–Vis pulsed irradiation at the nanosecond scale [6,19]. All

* Corresponding author. Dipartimento di Chimica, Università degli Studi di Pavia, Viale Taramelli 13, 27100, Pavia, Italy.
** Corresponding author. Dipartimento di Chimica, Universita degli Studi di of Milano, via Golgi 19, 20133, Milan, Italy.
*E-mail addresses:* martinailaria.fracchia@unipv.it (M. Fracchia), alberto.vertova@unimi.it (A. Vertova).

https://doi.org/10.1016/j.ijhydene.2025.02.265
Received 23 November 2024; Received in revised form 14 February 2025; Accepted 16 February 2025
Available online 21 February 2025

these studies relied on a common strategy: the selected material is studied with XAS to observe electronic changes between light and dark, using a suitable wavelength, under a bias potential. More recently, Chen's group, incorporating a semiconductor CdS/CdSe–$MoS_2$ and NiFe layered double hydroxide and using operando XAS at the Ni K edge, revealed that the light greatly promoted oxygen evolution reaction (OER) kinetics by forming more $Ni^{3+}/^{4+}$ active species [20].

On the other hand, investigations on pure semiconductors are more complex, because decoupling the absorption of visible and X-ray photons is not possible. Moreover, illumination and applied bias produce several effects in a semiconductor/electrolyte junction: charge separation, charge recombination, charge transfer at the interface [21,22]. This further complicates the investigation.

Indeed, XAS is capable of determining the oxidation state of an absorbing element, together with its local structure (coordination number and bond lengths), representing therefore the ideal tool for directly investigating the intermediate species forming upon illumination in a photoelectrochemical system [23]. In this sense, the encouraging example is the work by Braun et al., who studied α-$Fe_2O_3$ (hematite) photoanodes at the O–K edge (537 eV) and observed the accumulation and transfer of holes in dependence of the applied potential [24]. This seminal example suffers from the fact that O–K edge lies in the "soft" X-ray range, where the penetration depth is low, and this hinders the recording of XAS spectra under real operative conditions. Recently, Boscherini's group reported operando XAS study over $BiVO_4$ photoanode at the V K-edge and Bi $L_3$-edge. Bi $L_3$-edge was shifted to higher energy going from OCP to 1.85 V vs RHE, due to the removal of electrons from states at the top of the valence band, specifically those associated with O 2*p* and Bi 6*s* orbitals, resulting in a net decrease in the charge on Bi cations [25].

Here we present an operando study of two semiconductor photoelectrodes aiming at the direct observation of the intermediates forming under illumination. We do this in the case of copper(I) and copper(II) oxides, that are considered promising photocathodes being p-type semiconductors and suitable for hydrogen generation thanks to their favorable position of the relevant conduction band edges (−0.28 V *vs* SHE for CuO and −0.46 V for $Cu_2O$), that are more negative than the equilibrium potential for $H_2$ evolution [26,27]. Moreover, their low band gap energy (1.7 and 2.2 eV for CuO and $Cu_2O$, respectively) enables excitation by visible light [28]. They also present a wide range of applications in the environmental field, including ozone decomposition [29], degradation of contaminants [30], CO oxidation [31], $CO_2$ reduction [32]. These materials have been attracting attention because they are non-toxic and can be produced with easy synthetic protocols suitable for scalability [33–35]. In addition, copper is a highly abundant element. The major drawback lies in the poor stability of $Cu_2O$ and CuO in aqueous solution; in fact, the redox potentials of CuO to $Cu_2O$ or Cu lie within the band gap [36,37]. In a previous work, however, we observed that a copper oxide composite, $Cu_xO$, shows an outstanding stability, being able to retain photocurrent density of 0.4 mA $cm^{-2}$ for 5 h [38].

Broadly speaking, it was generally noticed that coupling $Cu_2O$ and CuO leads to an unexpected stability and long-term performances much higher than those achievable with the two pure semiconductors [39]. In this work both $Cu_2O$ and CuO were investigated through ex situ and operando XAS with the aim of elucidating their behavior and their stability under photo-electrochemical operative conditions. The results point to a complex relation of materials activity and stability in dependence on the applied potential, with marked difference depending on the nature of the pristine material. Moreover, in both materials, photogenerated charge carrier trapping was clearly observed by XAS. These findings allowed to shed light into the two photocathodes working mechanism, unravelling the reasons behind their favorable coupling. Finally, we believe that the presented approach could be conveniently extended to other photoelectrochemical systems for their better understanding towards a sustainable direct conversion of sunlight into solar fuels and chemicals.

## 2. Experimental

**Materials preparation**. $Cu_2O$ electrodes were prepared from a lactate-stabilized copper bath containing 0.2 M $CuSO_4$, 0.5 M $K_2HPO_4$ and 3 M lactic acid, whose pH is adjusted to 12 using 2 M KOH solution [40]. Electrochemical depositions were carried out by applying −0.4 V *vs.* SCE at 60 °C until the total amount of charge (1 C) is reached, using FTO as support. In this work an Au underlayer has been added, between the FTO surface and the $Cu_2O$ powder, by physical vapor deposition (PVD) (thickness of about 200 nm), to increase the adherence of the semiconductor and to stabilize it. These electrodes are labelled $Cu_2O$@Au@FTO and the characterization was reported in our previous paper [41]. CuO photoelectrodes have been prepared and characterized as reported previously [38]. Briefly, 100 μL of the suspension of freshly prepared nanocrystalline CuI in ethanol (3 mg $ml^{-1}$, 100 μL) were drop-casted on a FTO (Sigma Aldrich, surface resistivity ~7 Ω $m^2$) glass plate, previously washed with $H_2SO_4$, water and ethanol under ultrasounds. Subsequently, the electrodes were dried at room temperature and then annealed at 400 °C in air. For all prepared electrodes the exposed surface area was 1 $cm^2$.

**XAS measurements.** XAS measurements were performed in the fluorescence mode at the LISA beamline (BM08) at the European Synchrotron Radiation Facility (ESRF) at the Cu K-edge. A Si (111) double crystal monochromator was used; the harmonic rejection was realised by Pd mirrors with a cut-off energy of 20 keV, and a High Purity Germanium fluorescence detector array (13 elements) was used. The energy calibration was performed by measuring the absorption spectrum of metallic copper foil at the Cu K-edge (Cu–K: 8979 eV). The energy stability of the monochromator was checked by measuring the absorption spectrum of a Cu foil several times during the experiment and was always found to be better than ±0.05 eV. All data were obtained at room temperature. Spectra of standard samples CuO and $Cu_2O$, were acquired in the transmission mode. For the measurement, a proper amount of sample (as to give a unit jump in the absorption coefficient) was mixed to cellulose and pressed to pellet. The signal extraction was performed by means of the ATHENA code [42].

For the X-ray Absorption Near Edge Structure (XANES) analysis, the raw spectra were first background subtracted using a straight line and then normalized to unit absorption at 800 eV above the edge energy, where the EXAFS oscillations are not visible anymore. In this work, the quantitative determination of as as-prepared sample is possible by fitting the XANES with a linear combination fitting (LCF) of standard spectra of CuO, $Cu_2O$ and Cu. In the LCF, the XANES spectrum at a given edge in the target material is assumed to be reconstructed as the linear combination of the standard spectra. This is implemented in codes for the XAS data analysis [43], and has been extensively used in previous literature [44,45] and also by some Authors of the present group [46,47].

**FEXRAV.** In this recently introduced technique, X-ray energy is kept constant at a value at which the difference between the absorption coefficient of the selected atom at different oxidation states is at its maximum [48]. While the energy is constant, the applied potential is swept in the range of interest. FEXRAV experiments were carried out in dark or under illumination using a 400 nm light emitting diode (LED). The electrode potential was swept in the range given in figure captions, with a scan rate of 0.5 or 1 mV $s^{-1}$. For the measurements, a collection time of 10 s was used for each data point. As the CV lasted for 1600 s in the fastest cases, we can assume that the sample is not dynamically changing at a rate faster than our sampling probe. From the FEXRAV result, the fraction of $Cu_2O$ and CuO can be calculated, and the calculation details are shown in SI. For all the works discussed below, the selection of electrolyte pH was carefully optimized, with detailed procedures provided in the Supporting Information (Section 1.2).

$\Delta\mu$ spectra (light-dark) were collected at the Cu–K edge by setting the monochromator at the desired energy and then waiting for 30 s for stabilization. The point in dark conditions was acquired and the light

was subsequently switched on. After 30 s, the photocurrent was stable and the X-ray absorption under illumination was recorded. The light was then switched off and the whole sequence was repeated for each energy point. This system allows to record the spectra in dark and under illumination by nullifying any experimental artifact due to different monochromator conditions. For each polarization potential, we collected XANES spectra twice in light and in dark, we averaged them and then we calculated the $\Delta\mu$.

During XAS experiments, the photoelectrode potential was controlled by a CHI633D potentiostat/galvanostat (CH Instrument). All XANES and FEXRAV experiments were performed using a home-made cell shown in Fig. S1 and described in the SI. The illumination source was in all cases a 5 W 400 nm LED. Radiation damage was checked by performing control CV measurements after several hours of exposure to the X-rays during the XAS experiments. The close correspondence of the CV prior and after X-ray exposure allows to state that beam damage, if any, is not relevant in our case.

## 3. Results and discussion

### 3.1. FEXRAV – operando observation of photocathodes behavior

Considering copper oxide-based photocathodes in a photoelectrochemical water splitting system, we might expect three reactions to occur in parallel. These reactions are:

1) The electrochemical or photoelectrochemical reduction of water to hydrogen

$$H^+ + e^- \rightarrow \tfrac{1}{2}\, H_2 \; E^\circ = 0.00\ V \quad (1)$$

and,

2) the reduction of the photocathode material (parasitic processes),

$$2CuO + 2e^- + H_2O \rightarrow Cu_2O + 2OH^- \; E^\circ = 0.60\ V \quad (2a)$$

$$Cu_2O + 2e^- + H_2O \rightarrow 2Cu + 2OH^- \; E^\circ = 0.471\ V \quad (2b)$$

The possible disproportion reaction of $Cu_2O$, as described by Amano [49], here is not considered due to the co-presence of CuO and $Cu_2O$. Changes in the oxidation state occurring during the photoelectrochemical reaction can be directly monitored (in real time) using FEXRAV [11,48,50], that can be thus conveniently adopted to decouple the overall photocurrent from parasitic processes occurring at the photoelectrode. In FEXRAV, X-ray energy is fixed at a value where the difference between the absorption coefficient, $\mu$, of two or more standard phases is at its maximum. The choice is made after recording XANES spectra of standard materials. For Cu, $Cu_2O$ and CuO, this is shown in Fig. S4. In the present case, the energy of the incoming X-ray was alternatively fixed at 8981 eV giving the maximum contrast between the absorption coefficient ($\mu$) of $Cu_2O$ and CuO, or at 8979.1 eV, giving the maximum $\mu$ contrast between $Cu_2O$ and Cu. In this way, the electrode potential can be swept at will and any variation of $\mu$ indicates a change of the oxidation state of Cu. In both cases, we could attain a quantitative comparison between:

1) the degree of reduction (by FEXRAV): knowing the value of the absorption coefficients of the pure phases at the two selected X-ray energies (Fig. S4) and the relative change of $\mu$ during a FEXRAV experiment, it is possible to calculate the composition of the photoelectrodes during any potential scans.
2) the overall quantity of charge, obtained by integrating the current with time, that, for the sake of an easier comparison, will be here considered in first approximation fully due to the electrode material reduction.

With this strategy, 1) and 2) are immediately comparable. Obviously, if 2) exceeds 1), it is natural to conclude that the recorded current is not only caused by reactions (2a) or (2b), but also by reaction (1).

Fig. 1 shows the results of a FEXRAV experiment carried out in 0.5 M $Na_2HPO_4$ and 0.5 M NaOH (pH 11.1) on $Cu_2O$@Au@FTO at 8979.1 eV, both in the dark and under 400 nm illumination, which is the condition of highest photocurrent, thus causing the maximum perturbation on the Cu oxidation state transitions and local structure changes.

During this FEXRAV experiment, the electrode potential was swept in the dark in the first cycle and under illumination in the second one, and the results were illustrated in Fig. S5. As in this experiment the energy of the impinging X-ray beam is fixed to that of inflection point of the pre-edge peak of metallic Cu (8979.1 eV), and as at this energy the absorption of $Cu_2O$ is negligible (see Fig. S4), we can safely attribute any increase in $\mu$ to the reduction of the material (reaction 2b). Fig. 1 shows that, in the dark (a), the FEXRAV is constant, indicating a stable composition until *ca.* −0.3 V. When the potential is swept back, the FEXRAV signal starts to increase, indicating a reduction in the electrode material. The increase stops when the applied potential reaches 0 V. In the second cycle (light, Fig. 1b), the reduction starts at 0 V and eventually stabilizes. The current (black curve) shows a dramatic increase below 0 V, but above 0 V, where the FEXRAV signal is constant, a current of about −0.05 mA is observed in light. This photocurrent is not due to a reduction of the electrode, since the FEXRAV is flat in this range, but it should be rather attributed to the photogeneration of $H_2$. Overall, the amount of reduced $Cu_2O$, as obtained by FEXRAV, is very large under light, and eventually reaches 100%. The related trend of the total quantity of charge, obtained by integrating the current (blue dotted

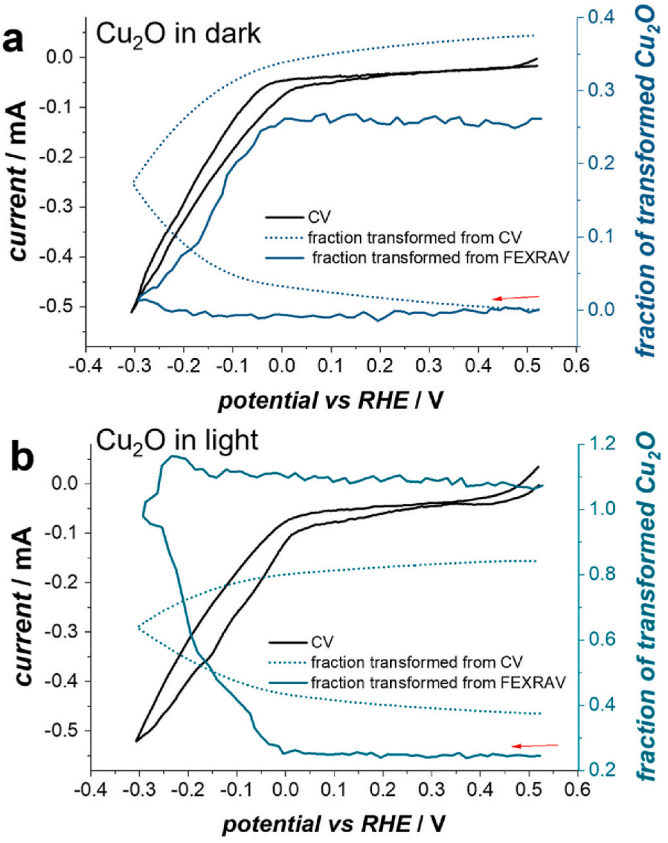


**Fig. 1.** Current intensity and fraction of $Cu_2O$ reduced to Cu as a function of the applied potential during a FEXRAV experiment on $Cu_2O$@Au@FTO electrode in 0.5 M $Na_2HPO_4$ + 0.5 M NaOH, pH 11 in the dark (a) and under LED illumination (b). Red arrows indicate the starting sweep potential. (For interpretation of the references to colour in this figure legend, the reader is referred to the Web version of this article.)

line), clarifies the stability/activity relation: in the dark, the quantity of charge rises immediately, much faster than FEXRAV, confirming $H_2$ evolution rather than CuO reduction (FEXRAV is flat). Under illumination, the integrated quantity of charge rises from the beginning but, starting from 0 V and together with FEXRAV, becoming steeper until the complete reduction of $Cu_2O$ to Cu. From these results, it is evident that $Cu_2O$ is indeed active towards $H_2$ evolution, but this occurs in parallel to a severe reduction of the electrode material to metallic copper. This observation serves as preliminary background for the study of CuO and explains the need of introducing a protecting semiconductor for $Cu_2O$.

FEXRAV on a CuO electrode was collected under illumination (Fig. 2a) by fixing the energy at 8981 eV, that is the pre-edge peak energy for $Cu_2O$. Quite interestingly, during the 1st cathodic scan (Fig. 2a, blue line) the CuO electrode is rapidly reduced (nearly 8% according to the FEXRAV), while during the 1st anodic scan only 2% of CuO is further reduced. Starting from the 3rd cycle, the reduced amount of CuO decreased, reaching an almost steady-state condition, indicating that the photocathode did not deteriorate any more (see blue curve in Fig. 2). On the contrary, the integration of CV current seems to point to a higher amount of Cu(II) reduction to Cu(I). However, this is only apparent, in fact the integration of CV current takes into account both the material reduction but also the $H_2$ evolution. Thus the combination of FEXRAV and CV measurements allows decoupling the two contributions. This can be done by calculating the $H_2$ to $Cu_2O$ ratio, see Fig. S6, as the ratio between the integration of CV current and the $Cu_2O$ amount determined by FEXRAV measurements. The $H_2/Cu_2O$ ratio reached almost a constant value of 4.5 starting from the 2nd cycle, indicating that mixed copper oxide is a stable photocathode. From this observation is possible to draw the following conclusions: (1) a $Cu_2O$ overlayer is formed in the 1st cathodic scan and it enhances the stability of the electrode; (2) the partial reduction of CuO to $Cu_2O$ is necessary to obtain an active and stable material towards $H_2$ production.

In order to further investigate the stability of the electrodes under operative conditions, XANES spectra were acquired at the Cu K-edge. $Cu_2O$ electrodes were first considered. As shown in our previous work [51], the performances of $Cu_2O$ electrodes can be enhanced by depositing $Cu_2O$ onto various underlayer materials, such as Au or Cu. It is worth noting that the underlayer, when present, has no significant influence on the resulting XAS spectrum: the ex-situ XANES spectra are shown in Fig. S7.

The stability of $Cu_2O$ samples under UV–Vis irradiation was first tested by recording XANES spectra of $Cu_2O$@Au@FTO before and after irradiation at $\lambda = 400$ nm for 10 h in absence of applied potential (open circuit). No change in composition is observed, meaning that the electrode is stable under illumination in 0.5 M $NaH_2PO_4$ + 0.5 M NaOH, pH 11.1 (see Fig. S8).

However, when the electrode is used as photocathode for $H_2$ evolution, significant changes in the composition are detected together with a drastic decrease of the photocurrent. The electrode was placed under operative condition ($E = 0.136$ V *vs.* RHE and under 400 nm LED illumination) until its photocurrent was reduced to 50% and then to 25% of its initial value. The ex-situ XANES spectra recorded after these treatments are displayed in Fig. 3; it is evident the marked difference at the pre-edge peak, that is shifted towards lower energies after use (compare blue and orange lines in the inset, displaying a magnification of the pre-

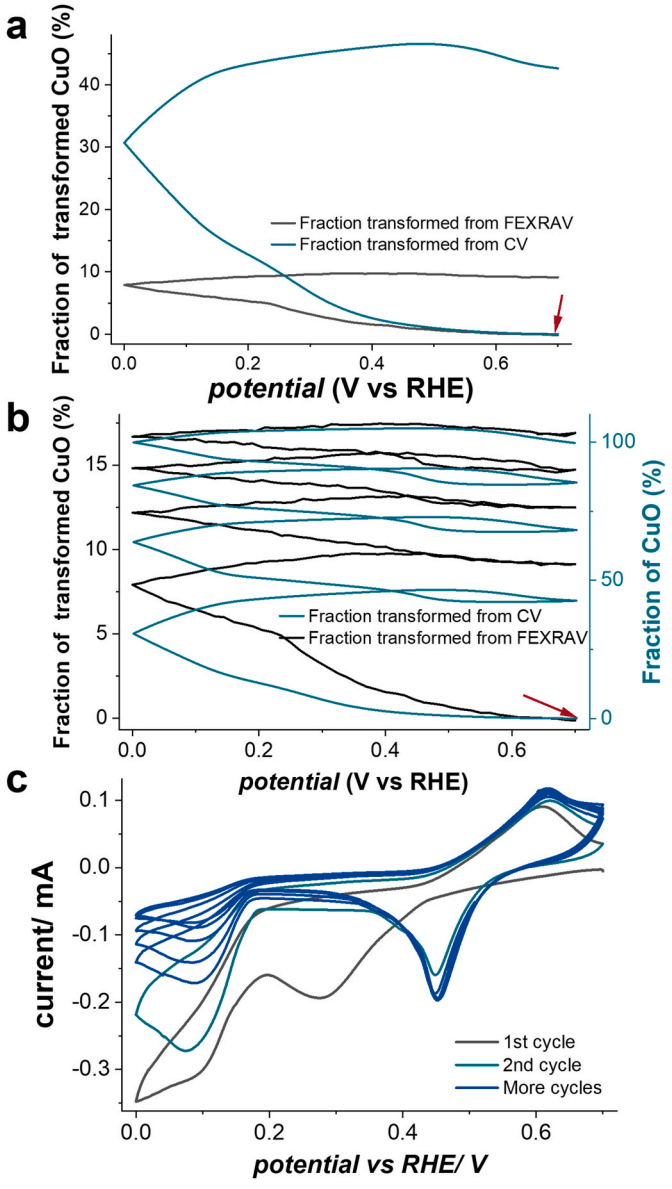


**Fig. 2.** (a) Fraction of reduced CuO obtained by first cycle of CV and corresponding FEXRAV at 8981 eV under LED 400 nm illumination (b) Fraction of reduced CuO obtained by four cycles of CV and corresponding FEXRAV at 8981 eV under LED 400 nm illumination (c) CVs in 0.1 M $K_2HPO_4 + KH_2PO_4$, pH = 7 electrolyte (the first cycle CV is in black, and the second cycle CV is in dark cyan, and the following cycles are in blue). (For interpretation of the references to colour in this figure legend, the reader is referred to the Web version of this article.)

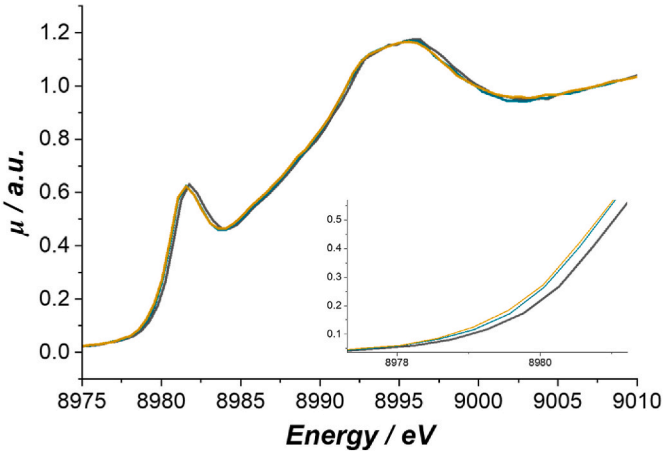


**Fig. 3.** XANES spectra of $Cu_2O$@Au@FTO as new (black line), after the 50% reduction of its initial photoactivity (blue line) and 75% of reduction (origin line, almost overlapped to the blue one). Photoelectrode degradation of electrode was performed in pH 11.1 electrolyte under 400 nm LED light and applied potential of 0.136V vs. RHE. Insert: magnification of pre-edge peak region. (For interpretation of the references to colour in this figure legend, the reader is referred to the Web version of this article.)

edge peak). This is a clear evidence of a partial reduction of $Cu_2O$ to Cu. The results indicate the formation of 8 ± 1% and 12 ± 2% of metallic Cu after 50% and 75% of photocurrent decrease, respectively, leading to a decrease in the photocurrent.

The behavior of CuO@FTO electrode is markedly different. As earlier reported [38], this material is initially composed only of pure CuO, whereas we observed that after 8 h at 0.3 V *vs* RHE and under chopped 400 nm illumination about the 70% of the initial CuO was reduced to $Cu_2O$. However, no metallic Cu was observed. This is very likely the reason for the improved stability observed for CuO with respect to $Cu_2O$: while the former maintains about 30% of its initial activity after 5h, the latter becomes inactive after a few minutes at moderate bias (between 0.6 and 0.3 V *vs* RHE).

### 3.2. Operando differential light-dark (Δμ) XANES spectra

In order to further investigate the nature and origin of photogenerated carriers, we recorded differential XANES spectra (under light at 400 nm and in dark, as described in the experimental section) under operative conditions. For both electrodes, $Cu_2O$@Au@FTO and CuO@FTO, these measurements were carried out at 0.49 V and 0.7 V *vs* RHE, respectively, where the stability of the electrodes is granted (in other words where the FEXRAV curve is flat, see Fig. 1a for $Cu_2O$@Au@FTO). The spectrum of the $Cu_2O$@Au@FTO electrode is shown in Fig. 4a. The Δμ signal has a low intensity, indicating that the differences between light and dark conditions are very small, apart from an evident positive peak around 8980 eV, in the region of the $Cu_2O$ pre-edge peak. As seen before, an increase of the absorption coefficient in this region can be symptomatic of the reduction of $Cu_2O$ to Cu. This effect has been highlighted both from the FEXRAV measurements and from the ex-situ measurements, evidencing that the photocatalytic activity leads to the formation of metallic copper on the electrode. It is therefore straightforward to compare the Δμ signal of Fig. 4a with the difference between the spectrum of the electrode spoilt until the decrease to 75% of its photoactivity and the spectrum of the pristine electrode. This difference is shown in Fig. 4b, where the two signals are on different y-axes (and scales) for better clarity: the two curves display a striking similarity, thus evidencing how, under illumination, a small quantity of metallic copper is formed. It can be therefore concluded that after the absorption of light at 400 nm, the electrons are partially trapped in the semiconductor, leading to the formation of Cu(0) sites. This happens since the reduction potential of $Cu_2O$ to Cu lies within the band gap, as already mentioned.

CuO@FTO has been characterized in the same way as the previously described Δμ experiment, polarizing the electrode at 0.7 V *vs.* RHE. In this case, three spectra were subsequently recorded as shown in Fig. 5, while the corresponding photocurrent is shown in Fig. S9. As seen before, the electrode undergoes a neat modification during the measurements, and the difference spectrum *Δμ* changes its shape from the first to the third measurement. The first spectrum shows that the material is almost fully made of CuO, with a small presence of $Cu_2O$, indicated by the feature at ca. 8981.5 eV.

The spectra in dark and light show a neat difference especially in correspondence of the white line. In particular, the spectrum obtained under illumination is positive in the whole range of energy from ca. 8980–9000 eV (see Fig. 5a). In order to understand the origin of this feature, we have to underline that the XANES spectrum of CuO when immersed in the electrolyte (see Fig. S10) shows a sizeable increase in the spectral weight in this energy region when compared to the spectrum of standard CuO. Multiple scattering calculations show that this region of the Cu–K XANES is very sensitive to distortion of the coordination around Cu; in particular, the spectral weight increases when the coordination octahedron in CuO is made less distorted. This effect is similar to that found for $Ni(OH)_2$ at the Ni–K edge [52]. Thus, the distortion of the $CuO_6$ octahedron in CuO decreases after immersion in the electrolytic solution and is further decreased after illumination. This

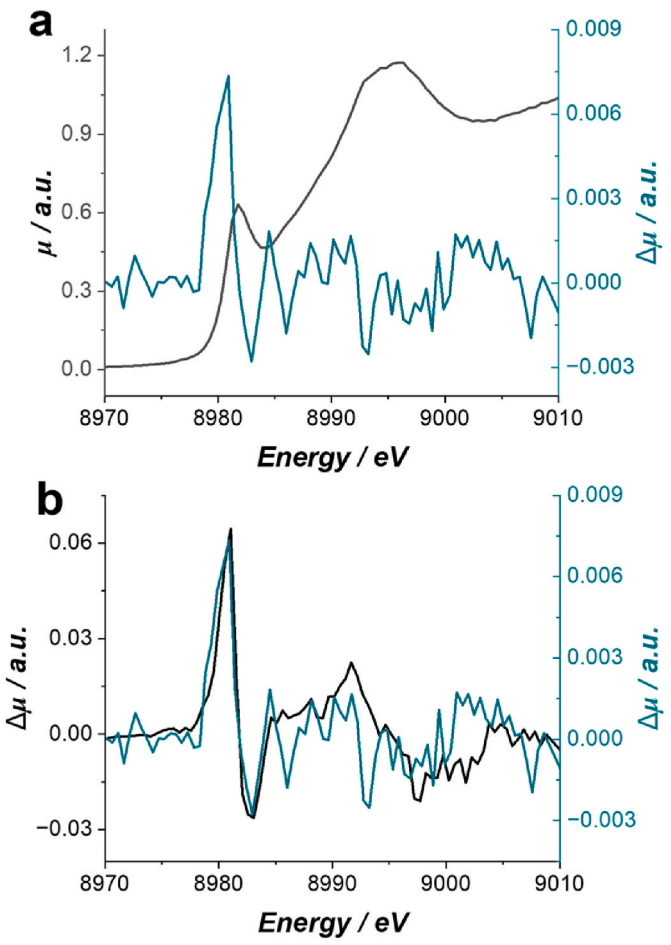


**Fig. 4.** (a) left y-axis: the XANES spectrum of the $Cu_2O$@Au@FTO, acquired in dark at 0.49 V vs RHE (black line). Right y: Δμ spectrum (the difference between light and dark, light - dark) (dark cyan line). (b) left y axis: comparison between Δμ spectrum of Fig. 4a (dark cyan line). Right y-axis: the difference between the ex-situ spectrum of pristine (black) and degraded at 75% $Cu_2O$@Au@FTO (origin). The two difference signals are plotted on two different y-axes for better clarity. (For interpretation of the references to colour in this figure legend, the reader is referred to the Web version of this article.)

is likely due to a modification of the material surface, that enriches in adsorbed –OH when immersed and further on during illumination [53]. However, when methanol, sacrificial hole scavenger, is added to the electrolyte large absorption coefficient differences are not visible, as shown in Fig. S11. Methanol, acting as scavenger, impedes the reaction:

$$H_2O + h^+ \rightarrow \bullet OH + H^+ \quad (4)$$

thus, reducing the white line difference between light and dark spectra [54]. Moreover, in case of illumination, the difference is not only positive in correspondence of the white line but also in correspondence of the edge (see Fig. 5a); this can also indicate the presence of a partial reduction to $Cu_2O$ under illumination, considering that the spectrum of $Cu_2O$ has a larger absorption coefficient with respect to the spectrum of CuO in this energy range. It is therefore likely that under illumination the material undergoes a reversible structural change and a partial reduction. The second and the third spectrum (Fig. 5b and c) show that during the measurements the electrode material is progressively reduced to $Cu_2O$ in agreement with the FEXRAV results and as indicated by the larger intensity of the feature at 8981.5 eV. A quantification of the formed $Cu_2O$ is possible through a linear combination fit starting from the spectrum of the pristine material (CuO@FTO) and the spectrum of standard $Cu_2O$, showing the formation of 18% and 25% of $Cu_2O$ for second and third XANES spectrum, respectively. The second and the

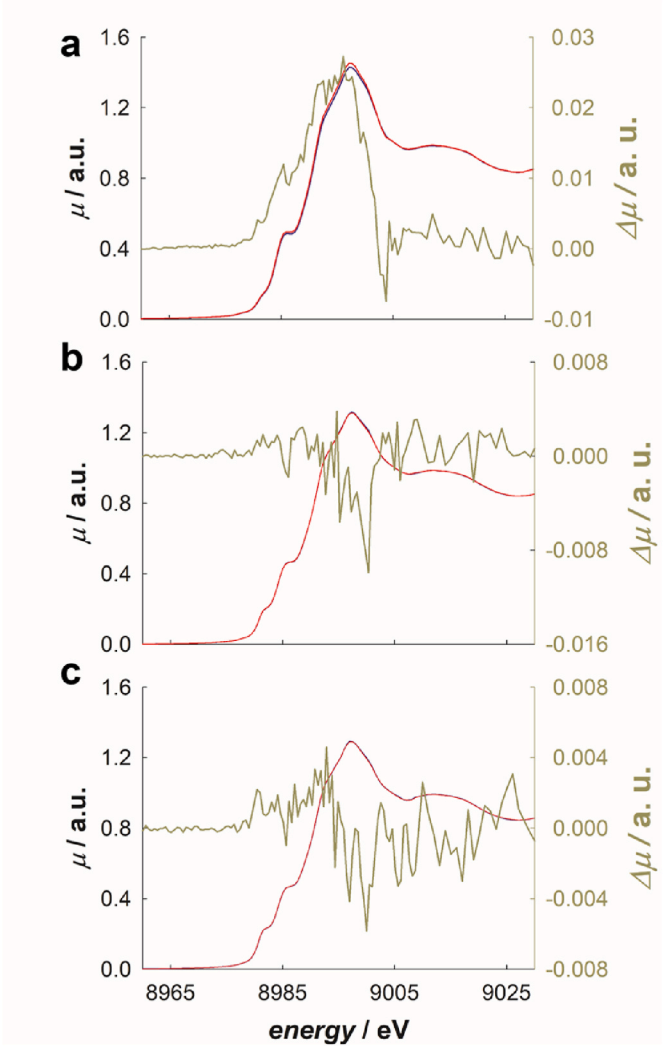


**Fig. 5.** Differential XANES spectra at the Cu K-edge recorded in dark (blue line) and light (red line) and corresponding $\Delta\mu$ difference (light – dark), indicated by the yellow line, for CuO@FTO electrode at 0.7 V in 0.1 M $K_2HPO_4$ + $KH_2PO_4$, pH = 7. The a, b and c panel indicate the three measurements acquired subsequently in time. (For interpretation of the references to colour in this figure legend, the reader is referred to the Web version of this article.)

third $\Delta\mu$ spectra show a similar trend, different from the first one. The intensity of the difference is much lower (especially for the last measurement), while the profile shows two distinct positive peaks centered at ca. 8982 eV and 8990 eV and a negative peak at ca. 9000 eV.

In Fig. 6, the $\Delta\mu$ signal obtained for the second measurement (Fig. 5b; yellow curve) is compared with the difference spectrum of $Cu_2O$ minus CuO standard samples (black curve). It can be observed that both the position of the features and the shape are coincident in the two cases, indicating the formation of $Cu_2O$ under illumination. However, two aspects should be underlined: i) as evidenced before, the broad peak at 9000 eV is not observed in the second and the third measurement. The decrease in CuO octahedron distortion probably occurs as a consequence of the interaction with the electrolyte and seems to be further enhanced by illumination. After the first measurement, however, a considerable layer of $Cu_2O$ is already formed on the electrode, thus preventing contact with the electrolyte. This can explain why this effect is not present in the last two $\Delta\mu$ difference spectra (Fig. 5b and c). ii) The relative intensity of the first two peaks is different in the second and the third measurement with respect to the difference of the $Cu_2O$ and CuO standards. Probably, along with a partial reversible reduction to $Cu_2O$, other

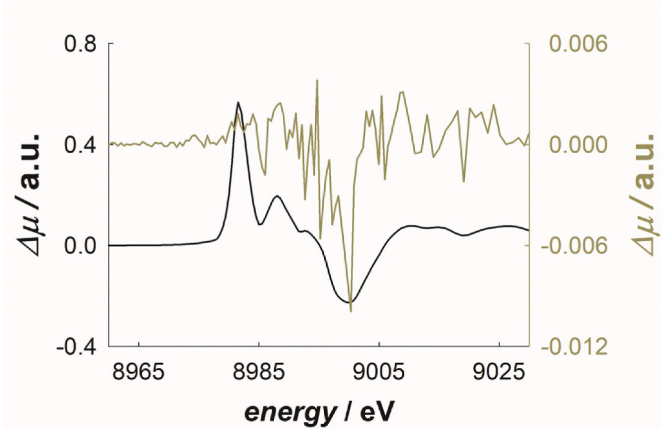


**Fig. 6.** Comparison of the second difference spectrum (yellow curve) and the difference of $Cu_2O$ minus CuO, obtained from the standard spectra (black curve). The two signals are plotted on different y-axes for better clarity. (For interpretation of the references to colour in this figure legend, the reader is referred to the Web version of this article.)

underlying processes occur as the effect of illumination.

## 4. Conclusions

In this work, the phase composition and stability of $Cu_2O$ and CuO-based photocathodes were addressed under operative conditions, using XAS-based techniques to investigate the performance of synthesized photocathodes for the photoelectrochemical water splitting process.

Firstly, FEXRAV and CV were carried out to detect the charge transfer during photoelectrochemical water splitting process over $Cu_2O$@Au@FTO and CuO@FTO photocathodes. The results reveal that $Cu_2O$ and CuO were both reduced during photoelectrochemical water splitting, as expecting since the reduction potentials of CuO and $Cu_2O$ lie within the band gap. While $Cu_2O$ irreversibly reduces to Cu(0), leading in turn to a drastic decrease of the photocurrent, CuO forms a favorable mixture of $Cu_2O$ and CuO. The presence of this mixed oxide is beneficial for the electrode performance, leading to a stable photocathode for PEC. Moreover, we remark that the combination of the two techniques: CV and FEXRAV is an effective strategy to decouple the current strictly connected with hydrogen evolution from that one due to powder degradation.

Notably, differential light-dark $\Delta\mu$ XANES were acquired at potentials where copper reduction in dark is not expected. Upon illumination both $Cu_2O$ and CuO are slightly reduced to metallic copper and Cu(I), respectively, indicating an electron trapping at the copper level. This highlighted again that a part of the photogenerated electrons are not involved in the $H_2$ production, but lead to the photocathode reduction. While this is detrimental in the case of $Cu_2O$, due to the formation of metallic Cu that reduces the light absorption, in the case of CuO it appears to be beneficial, for the formation of mixed oxides, as evidenced before.

Finally, these methods can provide an efficient way to investigate the photoelectrodes stability and chemical changes related to the formation of electron and hole pairs under illumination and in the presence of an electrode polarization.

## CRediT authorship contribution statement

**Xiufang He:** Writing – original draft, Software, Investigation, Data curation. **Tomasz Baran:** Writing – original draft, Methodology, Formal analysis, Data curation. **Martina Fracchia:** Writing – review & editing, Supervision, Resources, Methodology, Conceptualization. **Alberto Visibile:** Writing – original draft, Validation, Investigation, Data curation.

**Alberto Vertova:** Writing – review & editing, Validation, Supervision, Funding acquisition, Data curation, Conceptualization. **Paolo Ghigna:** Supervision, Methodology, Investigation, Conceptualization. **Alessandro Minguzzi:** Writing – review & editing, Supervision, Methodology, Funding acquisition, Conceptualization.

## Declaration of competing interest

The authors declare that they have no known competing financial interests or personal relationships that could have appeared to influence the work reported in this paper.

## Acknowledgements

The Authors are greatly indebted with Dr. Francesco D'Acapito for kind assistance in using the BM08 beamline and with the European Synchrotron Radiation Facility (beamline BM08 "LISA") for provision of beamtime (experiments 08-01-1004 and IH-EV-41).

A.M. is grateful to a project funded under the National Recovery and Resilience Plan (NRRP), Mission 4 Component 2 Investment 1.3 - Call for tender No. 1561 of 11.10.2022 of Ministero dell'Università e della Ricerca (MUR); funded by the European Union – NextGenerationEU Project code PE0000021, Concession Decree No. 1561 of 11.10.2022 adopted by Ministero dell'Università e della Ricerca (MUR), CUP D43C22003090001, Project title "Network 4 Energy Sustainable Transition – NEST".

This research is part of the project "One Health Action Hub: University Task Force for the resilience of territorial ecosystems", supported by Università degli Studi di Milano – PSR 2021 - GSA - Linea 6.

AV is grateful to Piano di Sostegno alla Ricerca 2022 (Linea 2A) – Università degli Studi di Milano.

M.F. and P.G. acknowledge support from the Ministero dell'Università e della Ricerca (MUR) and the University of Pavia through the program "Dipartimenti di Eccellenza 2023–2027".

## Appendix A. Supplementary data

Supplementary data to this article can be found online at https://doi.org/10.1016/j.ijhydene.2025.02.265.

## References

[1] Marwat MA, Humayun M, Afridi MW, Zhang H, Abdul Karim MR, Ashtar M, et al. Advanced catalysts for photoelectrochemical water splitting. ACS Appl Energy Mater 2021;4:12007–31. https://doi.org/10.1021/acsaem.1c02548.

[2] Al-Rasheidi M, Khan F, Khan MY, Khan A, Khan MT. Enhancements in PEC water splitting for sustainable hydrogen production using MnxCo0.015Zn1-xO bifunctional photocatalyst. Int J Hydrogen Energy 2024;93:1502–11. https://doi.org/10.1016/j.ijhydene.2024.11.054.

[3] Liu B, Wang X, Zhang Y, Xu L, Wang T, Xiao X, et al. A $BiVO_4$ photoanode with a $VO_x$ layer bearing oxygen vacancies offers improved charge transfer and oxygen evolution kinetics in photoelectrochemical water splitting. Angew Chem Int Ed 2023;62. https://doi.org/10.1002/anie.202217346.

[4] Bouwens T, Bakker TMA, Zhu K, Hasenack J, Dieperink M, Brouwer AM, et al. Using supramolecular machinery to engineer directional charge propagation in photoelectrochemical devices. Nat Chem 2023;15:213–21. https://doi.org/10.1038/s41557-022-01068-y.

[5] Minguzzi A, Naldoni A, Lugaresi O, Achilli E, D'Acapito F, Malara F, et al. Observation of charge transfer cascades in $\alpha$-$Fe_2O_3$/$IrO_x$ photoanodes by operando X-ray absorption spectroscopy. Phys Chem Chem Phys 2017;19:5715–20. https://doi.org/10.1039/C6CP08053G.

[6] Baran T, Fracchia M, Vertova A, Achilli E, Naldoni A, Malara F, et al. Operando and time-resolved X-ray absorption spectroscopy for the study of photoelectrode architectures. Electrochim Acta 2016;207:16–21. https://doi.org/10.1016/j.electacta.2016.04.153.

[7] Deng J, Zhang Q, Lv X, Zhang D, Xu H, Ma D, et al. Understanding photoelectrochemical water oxidation with X-ray absorption spectroscopy. ACS Energy Lett 2020;5:975–93. https://doi.org/10.1021/acsenergylett.9b02757.

[8] Ismail ASM, Garcia-Torregrosa I, Vollenbroek JC, Folkertsma L, Bomer JG, Haarman T, et al. Detection of spontaneous FeOOH formation at the hematite/Ni(Fe)OOH interface during photoelectrochemical water splitting by operando X-ray absorption spectroscopy. ACS Catal 2021;11:12324–35. https://doi.org/10.1021/acscatal.1c02566.

[9] Arul KT, Nga TTT, Dong C, Chou W. Advanced X-ray absorption spectroscopy on electrocatalysts and photocatalysts. Water Photo- and Electro-Catalysis 2024:363–95. https://doi.org/10.1002/9783527831005.ch10. Wiley.

[10] Zoric MR, Basera P, Palmer LD, Aitbekova A, Powers-Riggs N, Lim H, et al. Oxidizing role of Cu cocatalysts in unassisted photocatalytic $CO_2$ reduction using p-GaN/$Al_2O_3$/Au/Cu heterostructures. ACS Nano 2024;18:19538–48. https://doi.org/10.1021/acsnano.4c02088.

[11] Malara F, Fracchia M, Kmentová H, Psaro R, Vertova A, Oliveira de Souza D, et al. Direct observation of photoinduced higher oxidation states at a semiconductor/electrocatalyst junction. ACS Catal 2020;10:10476–87. https://doi.org/10.1021/acscatal.0c02789.

[12] Loyola CZ, Zitolo A, Troncoso N, Carrasco J, Choque S, Abarca G, et al. High content Fe(III) electrocatalyst for the oxygen reduction and evolution reactions. Spectroscopic, electrochemical, and theoretical insights. Int J Hydrogen Energy 2025;101:605–16. https://doi.org/10.1016/j.ijhydene.2024.12.385.

[13] Fracchia M, Cristino V, Vertova A, Rondinini S, Caramori S, Ghigna P, et al. Operando X-ray absorption spectroscopy of WO3 photoanodes. Electrochim Acta 2019;320:134561. https://doi.org/10.1016/j.electacta.2019.134561.

[14] Timoshenko J, Roldan Cuenya B. *In situ/operando* electrocatalyst characterization by X-ray absorption spectroscopy. Chem Rev 2021;121:882–961. https://doi.org/10.1021/acs.chemrev.0c00396.

[15] Lin S-C, Chang C-C, Chiu S-Y, Pai H-T, Liao T-Y, Hsu C-S, et al. Operando time-resolved X-ray absorption spectroscopy reveals the chemical nature enabling highly selective CO2 reduction. Nat Commun 2020;11:3525. https://doi.org/10.1038/s41467-020-17231-3.

[16] Spanu D, Minguzzi A, Recchia S, Shahvardanfard F, Tomanec O, Zboril R, et al. An operando X-ray absorption spectroscopy study of a NiCu−$TiO_2$ photocatalyst for $H_2$ evolution. ACS Catal 2020;10:8293–302. https://doi.org/10.1021/acscatal.0c01373.

[17] Braglia L, Fracchia M, Ghigna P, Minguzzi A, Meroni D, Edla R, et al. Understanding solid–gas reaction mechanisms by operando soft X-ray absorption spectroscopy at ambient pressure. J Phys Chem C 2020;124:14202–12. https://doi.org/10.1021/acs.jpcc.0c02546.

[18] Tsyganok A, Ghigna P, Minguzzi A, Naldoni A, Murzin V, Caliebe W, et al. Operando X-ray absorption spectroscopy (XAS) observation of photoinduced oxidation in FeNi (Oxy)hydroxide overlayers on hematite ($\alpha$-$Fe_2O_3$) photoanodes for solar water splitting. Langmuir 2020;36:11564–72. https://doi.org/10.1021/acs.langmuir.0c02065.

[19] Fracchia M, Ghigna P, Vertova A, Rondinini S, Minguzzi A. Time-resolved X-ray absorption spectroscopy in (Photo)Electrochemistry. Surfaces 2018;1:138–50. https://doi.org/10.3390/surfaces1010011.

[20] Wu Z, Liu X, Li H, Sun Z, Cao M, Li Z, et al. A semiconductor-electrocatalyst nano interface constructed for successive photoelectrochemical water oxidation. Nat Commun 2023;14:2574. https://doi.org/10.1038/s41467-023-38285-z.

[21] Vecchi P, Piccioni A, Mazzaro R, Mazzanti M, Cristino V, Caramori S, et al. Charge separation efficiency in $WO_3$/$BiVO_4$ photoanodes with CoFe prussian blue catalyst studied by wavelength-dependent intensity-modulated photocurrent spectroscopy. Sol RRL 2022;6. https://doi.org/10.1002/solr.202200108.

[22] Liu X, Pan J, Huang H, Zhang X, Sun N, Gu C, et al. The advanced development of floatable photocatalysts: preparation, advantages, and application. Chem Eng J 2023;476:146868. https://doi.org/10.1016/j.cej.2023.146868.

[23] Guan W, Cheng W, Pei S, Chen X, Yuan Z, Lu C. Probing coordination number of single-atom catalysts by *d* -band center-regulated luminescence. Angew Chem 2024;136:20240121. https://doi.org/10.1002/ange.202401214.

[24] Braun A, Sivula K, Bora DK, Zhu J, Zhang L, Grätzel M, et al. Direct observation of two electron holes in a hematite photoanode during photoelectrochemical water splitting. J Phys Chem C 2012;116:16870–5. https://doi.org/10.1021/jp304254k.

[25] Piccioni A, Kopula Kesavan J, Amidani L, Mazzaro R, Berardi S, Caramori S, et al. Operando double-edge high-resolution X-ray absorption spectroscopy study of $BiVO_4$ photoanodes. J Synchrotron Radiat 2024;31:464–8. https://doi.org/10.1107/S1600577524002741.

[26] Zhong X, Li L, Li C, Mu X, Cui A, Shan G. Cu ions intercalated GO/Cu2O photocathode-enabled promotion on charge separation and transfer for efficient photoelectrochemical water splitting. J Alloys Compd 2023;969:172432. https://doi.org/10.1016/j.jallcom.2023.172432.

[27] Heo J, Bae H, Mane P, Burungale V, Seong C, Ha J-S. Surface engineering of $Cu_2O$ photocathodes via facile graphene oxide decoration for improved photoelectrochemical water splitting. ACS Omega 2023;8:32794–803. https://doi.org/10.1021/acsomega.3c03585.

[28] Baran T, Visibile A, Busch M, He X, Wojtyla S, Rondinini S, et al. Copper oxide-based photocatalysts and photocathodes: fundamentals and recent advances. Molecules 2021;26:7271. https://doi.org/10.3390/molecules26237271.

[29] Wang A, Guan J, Zhang L, Wang H, Ma G, Fan G, et al. In situ synthesis of monolithic $Cu_2O$–CuO/Cu catalysts for effective ozone decomposition. J Phys Chem C 2022;126:317–25. https://doi.org/10.1021/acs.jpcc.1c10208.

[30] Serrà A, Gómez E, Michler J, Philippe L. Facile cost-effective fabrication of Cu@Cu2O@CuO–microalgae photocatalyst with enhanced visible light degradation of tetracycline. Chem Eng J 2021;413:127477. https://doi.org/10.1016/j.cej.2020.127477.

[31] Shi Y, Xu L, Chen M, Yang B, Cheng G, Wu C, et al. Fabricating Cu2O-CuO submicron-cubes for efficient catalytic CO oxidation: the significant effect of heterojunction interface. J Ind Eng Chem 2022;105:324–36. https://doi.org/10.1016/j.jiec.2021.09.031.

[32] Luévano-Hipólito E, Torres-Martínez LM, alejandro Ávila-López M. Visible-light-driven CO2 reduction and H2 evolution boosted by 1D Cu2O/CuO

heterostructures. J Phys Chem Solid 2022;170:110924. https://doi.org/10.1016/j.jpcs.2022.110924.
[33] Feng C, Zhang C, Xu C, Lin S, Zhang B, Wu H, et al. A room-temperature ppb-level H2S sensor based on MoO3/CuO/g-C3N4 via a simple synthesis. Sens Actuators B Chem 2023;374:132827. https://doi.org/10.1016/j.snb.2022.132827.
[34] Sondors R, Gavars D, Spalva E, Kons A, Lohmus R, Volkova M, et al. Synthesis and enhanced room-temperature thermoelectric properties of CuO–MWCNT hybrid nanostructured composites. Nanoscale Adv 2024;6:697–704. https://doi.org/10.1039/D3NA00888F.
[35] Zhang Y, Lin Z, Duan S, Yuan Y, Song A, Ma Y. Spectroelectrochemical identification of CuO impurities catalyzing water reduction on CuBi2O4 photocathodes. ACS Energy Lett 2024;9:1761–70. https://doi.org/10.1021/ACSENERGYLETT.4C00399/ASSET/IMAGES/LARGE/NZ4C00399_0005.JPEG.
[36] Tilley SD. Will cuprous oxide really make it in water-splitting applications? ACS Energy Lett 2023;8:2338–44. https://doi.org/10.1021/acsenergylett.3c00578.
[37] Ranjan AK, Jha PK, Jha PA, Singh P. Catalyzing hydrogen production: exploring plasmonic effects in self-assembled CuO/Cu2O thin films via pulsed laser deposition. J Appl Phys 2024;135. https://doi.org/10.1063/5.0188802.
[38] Baran T, Wojtyła S, Lenardi C, Vertova A, Ghigna P, Achilli E, et al. An efficient Cu $_x$ O photocathode for hydrogen production at neutral pH: new insights from combined spectroscopy and electrochemistry. ACS Appl Mater Interfaces 2016;8:21250–60. https://doi.org/10.1021/acsami.6b03345.
[39] John S, Roy SC. CuO/Cu2O nanoflake/nanowire heterostructure photocathode with enhanced surface area for photoelectrochemical solar energy conversion. Appl Surf Sci 2020;509:144703. https://doi.org/10.1016/j.apsusc.2019.144703.
[40] Achilli E, Vertova A, Visibile A, Locatelli C, Minguzzi A, Rondinini S, et al. Structure and stability of a copper(II) lactate complex in alkaline solution: a case study by energy-dispersive X-ray absorption spectroscopy. Inorg Chem 2017;56:6982–9. https://doi.org/10.1021/acs.inorgchem.7b00553.
[41] Visibile A, Fracchia M, Baran T, Vertova A, Ghigna P, Ahlberg E, et al. Electrodeposited Cu thin layers as low cost and effective underlayers for Cu2O photocathodes in photoelectrochemical water electrolysis. J Solid State Electrochem 2020;24:339–55. https://doi.org/10.1007/s10008-019-04441-z.
[42] Newville M. Fundamentals of XAFS. Rev Mineral Geochem 2014;78:33–74. https://doi.org/10.2138/rmg.2014.78.2.
[43] Ravel B, Newville M. ATHENA, artemis, hephaestus: data analysis for X-ray absorption spectroscopy using IFEFFIT. J Synchrotron Radiat 2005;12:537–41. https://doi.org/10.1107/S0909049505012719.
[44] Rockenberger J, Zum Felde U, Tischer M, Tröger L, Haase M, Weller H. Near edge X-ray absorption fine structure measurements (XANES) and extended x-ray absorption fine structure measurements (EXAFS) of the valence state and coordination of antimony in doped nanocrystalline SnO2. J Chem Phys 2000;112:4296–304. https://doi.org/10.1063/1.480975.
[45] Kim WB, Choi SH, Lee JS. Quantitative analysis of Ti-O-Si and Ti-O-Ti bonds in Ti-Si binary oxides by the linear combination of XANES. https://doi.org/10.1021/JP000042; 2000.
[46] Abudukade MT, Pinna M, Spanu D, De Amicis G, Minguzzi A, Vertova A, et al. In situ X-ray absorption spectroscopy study of the deactivation mechanism of a Ni-SrTiO3 photocatalyst slurry active in water splitting. J Phys Chem C 2024;128:48. https://doi.org/10.1021/ACS.JPCC.4C04688/ASSET/IMAGES/LARGE/JP4C04688_0008.JPEG.
[47] Spanu D, Minguzzi A, Recchia S, Shahvardanfard F, Tomanec O, Zboril R, et al. An operando X-ray absorption spectroscopy study of a NiCu−TiO $_2$ photocatalyst for H $_2$ evolution. ACS Catal 2020;10:8293–302. https://doi.org/10.1021/acscatal.0c01373.
[48] Minguzzi A, Lugaresi O, Locatelli C, Rondinini S, D'Acapito F, Achilli E, et al. Fixed energy X-ray absorption voltammetry. Anal Chem 2013;85:7009–13. https://doi.org/10.1021/ac401414v.
[49] Amano F, Ebina T, Ohtani B. Enhancement of photocathodic stability of p-type copper(I) oxide electrodes by surface etching treatment. Thin Solid Films 2014;550:340–6. https://doi.org/10.1016/j.tsf.2013.10.122.
[50] Minguzzi A, Lugaresi O, Achilli E, Locatelli C, Vertova A, Ghigna P, et al. Observing the oxidation state turnover in heterogeneous iridium-based water oxidation catalysts. Chem Sci 2014;5. https://doi.org/10.1039/c4sc00975d.
[51] Visibile A, Fracchia M, Baran T, Vertova A, Ghigna P, Ahlberg E, et al. Electrodeposited Cu thin layers as low cost and effective underlayers for Cu2O photocathodes in photoelectrochemical water electrolysis. J Solid State Electrochem 2020;24:339–55. https://doi.org/10.1007/s10008-019-04441-z.
[52] Alp EE, Shenoy GK, Hinks DG, II DWC, Soderholm L, Schuttler H-B, et al. Determination of valence of Cu in superconducting La(2-x)(Sr,Ba)xCuO4. Phys Rev B 1987;35:7199–202. https://doi.org/10.1103/PhysRevB.35.7199.
[53] Meroni D, Lo Presti L, Di Liberto G, Ceotto M, Acres RG, Prince KC, et al. A close look at the structure of the TiO $_2$ -APTES interface in hybrid nanomaterials and its degradation pathway: an experimental and theoretical study. J Phys Chem C 2017;121:430–40. https://doi.org/10.1021/acs.jpcc.6b10720.
[54] Siavash Moakhar R, Hosseini-Hosseinabad SM, Masudy-Panah S, Seza A, Jalali M, Fallah-Arani H, et al. Photoelectrochemical water-splitting using CuO-based electrodes for hydrogen production: a review. Adv Mater 2021;33. https://doi.org/10.1002/adma.202007285.